OFFICE OF NAVAL RESEARCH

Contract N0014-86-K-0191

R & T Code 431a010

Technical Report No. 2

# FRACTOGRAPHIC ANALYSIS OF CVD ZnS

by

P. L. Yoder and J. J. Mecholsky



July 11, 1988

The Pennsylvania State University
Departments of Chemistry and Materials Science and Engineering
University Park, PA 16802

SECURITY CLASSIFICATION OF THIS PAGE

# REPORT DOCUMENTATION PAGE

| | |
|---|---|
| 1a. REPORT SECURITY CLASSIFICATION | 1b RESTRICTIVE MARKINGS |
| 2a. SECURITY CLASSIFICATION AUTHORITY | 3. DISTRIBUTION/AVAILABILITY OF REPORT<br>Approved for Public Release<br>Distribution Unlimited |
| 2b. DECLASSIFICATION/DOWNGRADING SCHEDULE | |
| 4. PERFORMING ORGANIZATION REPORT NUMBER(S)<br>#2 | 5. MONITORING ORGANIZATION REPORT NUMBER(S)<br>N0014-86-K0191 |
| 6a. NAME OF PERFORMING ORGANIZATION<br>The Pennsylvania State University<br>6b. OFFICE SYMBOL (If applicable) | 7a. NAME OF MONITORING ORGANIZATION<br>Office of Naval Research<br>Dr. R. Schwartz |
| 6c. ADDRESS (City, State, and ZIP Code) | 7b. ADDRESS (City, State, and ZIP Code)<br>Code 3854<br>Naval Weapons Center<br>China Lake, CA 93555 |
| 8a. NAME OF FUNDING/SPONSORING ORGANIZATION<br>8b. OFFICE SYMBOL (If applicable) | 9. PROCUREMENT INSTRUMENT IDENTIFICATION NUMBER |
| 8c. ADDRESS (City, State, and ZIP Code) | 10. SOURCE OF FUNDING NUMBERS<br>PROGRAM ELEMENT NO. / PROJECT NO. / TASK NO. / WORK UNIT ACCESSION NO. |

11. TITLE (Include Security Classification)

Fractographic Analysis of CVD ZnS .

12. PERSONAL AUTHOR(S)
P. L. Yoder and J. J. Mecholsky

| 13a. TYPE OF REPORT | 13b. TIME COVERED | 14. DATE OF REPORT (Year, Month, Day) | 15. PAGE COUNT |
|---|---|---|---|
| Technical | FROM _____ TO _____ | 1988, July 11 | 21 |

16. SUPPLEMENTARY NOTATION

| 17. COSATI CODES | | | 18. SUBJECT TERMS (Continue on reverse if necessary and identify by block number) |
|---|---|---|---|
| FIELD | GROUP | SUB-GROUP | |
| | | | |
| | | | |

19. ABSTRACT (Continue on reverse if necessary and identify by block number)

The fracture surfaces of chemically vapor deposited (CVD) zinc sulfide bars obtained from Raytheon were examined to determine the size of characteristic features surrounding the fracture initiating cracks known as mirror, mist, and hackle. The critical stress intensity factor or fracture toughness, which is a measure of the resistance to fracture was determined from fracture mechanics equations to be 1.1 ± 0.1 $MPam^{1/2}$ and from fracture surface analysis to be 1.04 ± 0.03 $MPam^{1/2}$. Statistically there is no difference between these values indicating there are no local residual stresses at the crack tip. The mirror "constants" were established to be $M_1$ = 2.1 $MPam^{1/2}$, $M_2$ = 2.8 $MPam^{1/2}$, $M_3$= 3.7 $MPam^{1/2}$. The branching stress intensity factors are: $K_1$ = 3.1 $MPam^{1/2}$, $K_2$ = 4.0 $MPam^{1/2}$, and $K_3$ = 5.2 $MPam^{1/2}$.

| 20 DISTRIBUTION/AVAILABILITY OF ABSTRACT | 21. ABSTRACT SECURITY CLASSIFICATION | |
|---|---|---|
| ☐ UNCLASSIFIED/UNLIMITED ☐ SAME AS RPT. ☐ DTIC USERS | | |
| 22a NAME OF RESPONSIBLE INDIVIDUAL | 22b TELEPHONE (Include Area Code) | 22c OFFICE SYMBOL |

DD FORM 1473, 84 MAR — 83 APR edition may be used until exhausted. All other editions are obsolete.

SECURITY CLASSIFICATION OF THIS PAGE

*U.S. Government Printing Office: 1985—507-045

## SUMMARY

The fracture surfaces of chemically vapor deposited (CVD) zinc sulfide bars obtained from Raytheon were examined to determine the size of characteristic features surrounding the fracture initiating cracks known as mirror, mist, and hackle. The critical stress intensity factor or fracture toughness, which is a measure of the resistance to fracture was determined from fracture mechanics equations to be $1.1 \pm 0.1$ MPam$^{1/2}$ and from fracture surface analysis to be $1.04 \pm 0.03$ MPam$^{1/2}$. Statistically there is no difference between these values indicating there are no local residual stresses at the crack tip. The mirror "constants" were established to be $M_1 = 2.1$ MPam$^{1/2}$, $M_2 = 2.8$ MPam$^{1/2}$, $M_3 = 3.7$ MPam$^{1/2}$. The branching stress intensity factors are: $K_1 = 3.1$ MPam$^{1/2}$, $K_2 = 4.0$ MPam$^{1/2}$, and $K_3 = 5.2$ MPam$^{1/2}$.


## INTRODUCTION

Chemically vapor deposited (CVD) zinc sulfide is used as an infrared transmitting window on heat-seeking missiles and laser systems. In many of these in-service environments, mechanical and thermal stresses can lead to crack growth and fracture. Thus, a knowledge of the mechanical and thermal properties of these materials is necessary. Although many investigations and research papers have concentrated on the processing and properties of ZnS material, very little has been written on the characterization of the fracture surface of ZnS.

This report is written to demonstrate the techniques of determining the fracture origin and the surrounding topography. The fracture toughness, or resistance to crack propagation, is determined from fracture surface features. Their values compare well with reported values. More importantly, observation of the fracture surface provides a tool by which we can determine the state of stress, identify the fracture origin, and analyze the fracture process.

## EXPERIMENTAL PROCEDURE

Fracture bars of polycrystalline ZnS and the corresponding strength data were received from Raytheon for fractographic analysis. The bars measured approximately

89mm x 8.3mm x 12.8mm and were prepared by CVD. The bars were tested using four point flexure with inner and outer spans of 25.4mm and 50.8mm, respectively. Fracture surfaces were first evaluated using a polarizing light microscope (PLM) where fracture origins and surrounding topography were located and measured. Fracture markings such as "river" markings, cleavage steps, and crack front profiles on individual grains were helpful in tracing the fracture path back to the origin of failure.[1] Fracture surfaces were then examined on a SEM where the depth of field was utilized to obtain fractographs and validate the measurements of boundaries obtained on the PLM.

## BACKGROUND

Failure of brittle materials is initiated by defects in the bulk or on the surface of the material. Since many advanced materials are now prepared to a degree where pores and inclusions are virtually eliminated, it is often machining or polishing flaws on the surface which cause failure. Although these flaws can take on irregular shapes, they can be modeled as semielliptical in geometry.

For a semielliptical crack of depth a and half-width b, the equivalent semi-circular crack, c, is given by:

$$c = \sqrt{ab} \qquad 1)$$

It has been shown that for a surface flaw without local residual stresses which is subjected to an applied stress normal to the plane of the defect, one can relate the size of the defect, c, and the failure stess, $\sigma$, to the critical stress intensity factor or fracture toughness, $K_{IC}$, of the material by:[2,3]

$$K_{IC} = \frac{\sqrt{(1.2\pi)}\sigma\sqrt{c}}{\phi} \qquad 2)$$

The elliptical integral of the second kind, $\phi$, accounts for the degree of ellipticity of the flaw. For a semi-circular surface flaw $\phi = 1.57$ and Equation 2) becomes:[3,4,5]

$$K_{IC} = 1.24\sigma\sqrt{c} \qquad 3)$$

The fracture surface of brittle materials exhibits distinct fracture markings (boundaries) beyond the region of the critical flaw. These boundaries can be used to quantitatively describe the stress state of a material through fracture mechanics principles. There are four distinct regions (three boundaries) which surround the critical flaw (Fig. 1). As a crack propagates from the critical flaw, a " smooth" region known as the (fracture) "mirror is formed. The fracture mirror is surrounded by a region of small radial ridges known as mist and this by of an even rougher radial ridge region known as hackle. Finally, as the propagating crack reaches a characteristic critical stress intensity, a region known as macroscopic crack branching occurs. This is a region where two of more cracks form the primary crack. The distance measured along the tensile surface from the start of the propagating critical flaw (usually at one edge) to the boundary ot the mirror/mist region (inner mirror radius, $r_1$), of the mist/hackle (outer mirror radius, $r_2$), and of the hackle/crack branching region (crack branching radius, $r_3$) have been shown to be empirically related to the fracture stress, $\sigma$, by the following:[5,6]

$$\sigma r^{1/2} = M_j \text{ (constant)} \qquad 4)$$

where j = 1, 2, or 3 for the mirror /mist, mist/hackle, and crack branching boundaries, respectively; $M_j$ is the corresponding mirror constant. The mirror constants are proportional to the stress intensity at the point of a particular boundary.

Equations 3 and 4 can be combined to obtian an expression for the critical stress intensity factor from fractographic data:[5,6]

$$K_{IC} = 1.24(c/r_j)^{1/2}M_j \qquad 5)$$

where $(c/r_j)$ is the flaw size to mirror size ratio and is constant for a given material. If the mirror "constant ", $M_j$, of a particular material is known, the stress intensity at that boundary, $K_j$, can be calculated. Kirchner and Kirchner[7] have shown that the mirror radii occur at characteristic stress intensities described by the following equation:

$$K_j = [2/\pi^{1/2}]Q\sigma r_j^{1/2} \qquad 6)$$

where Q is the value of $K_I/K_{IC}$ needed to correct $K_{IC}$ for an internal penny-shaped crack to obtain the stress intensity factor for a semi-circular surface crack.[7] Thus, Equations 5 and 6 are identical for measurements along the tensile surface, if $M_j = 0.7K_j$. However, $K_j$ is constant everywhere along the "mirror" boundaries.

## RESULTS AND DISCUSSION

Fracture surfaces of CVD ZnS were examined with a polarizing light microscope and a scanning electron microscope for fracture markings shown schematically in Figure 1. Representative fracture surfaces for ZnS can be seen in Figures 2, 3, and 4. On observation of the samples, the fracture boundaries where located and measured, Table 1. The boundaries measured include: the depth (a) and half-width (b) of the critical flaw (c), the (mirror/mist) inner mirror radius ($r_1$), the (mist/hackle) outer mirror radius ($r_2$), and the crack branching radius ($r_3$). Using the depth and half-width of the critical flaw, the size of the critical flaw, c, was calculated through Equation 1 and is also listed in Table 1.

It can be seen from Table 1 that the size of the critical flaw ranged from 46μm - 103μm. It should also be noted that certain fracture boundaries could not be

determined since they were lost during the fracture process.. On observation of the fracture surfaces, it was found that the inner mirror radius was not nearly as distinguishable as were the other fracture boundaries. This is often the case for polycrystalline ceramics.[2] All the critical flaws located on the fracture surfaces appeared to be the result of machining or handling, i.e., surface damage.[4]

The fracture boundary measurements given in Table 1 were used with fracture mechanics equations to determine $K_{IC}$ (Eqs. 3 and 5). Using the fracture stress and size of the measured critical flaw, $K_{IC}$ was determined from Equation 3 (Table 2). It can be seen from Table 2 that the average fracture toughness was $1.1 \pm 0.1$ MPam$^{1/2}$. This is in agreement with the 1.0 MPam$^{1/2}$ value reported.[8] Thus, fractography can be used as an independent method for determining the fracture toughness of this material.

Using the measurements determined for mirror radii, the corresponding mirror constants were calculated from Equation 4 and are listed in Table 3. The mirror constants shown in Table 3 are material constants for measurements along the tensile surface and are directly proportional to the stress intensity at these points. The branching stress intensities at these points (i.e., the inner mirror, outer mirror, and crack branching distances) were calculated from Equation 6 and are give in Table 4. These stress intensities are constant along the entire mirror boundary for a given material. The mirror "constants" or branching stress intensities are established so that they can used later to determine the stress at failure for research, production, or in-service failure analysis.

In order to normalize the strength for different flaw sizes, mirror radii to flaw size ratios were calculated (Table 5) and an average of these values was used to calculate the critical stess intensity factor from Equation 5 (Table 6). It can be seen from Table 6 that the values determined in this manner agree very will with the $K_{IC}$ values shown in Table 2. The agreement between these two techniques indicates that there are no local residual stresses on the fracture initiating crack. If there were local residual streses present, the value for $K_{IC}$ obtained by the two techniques would be different.

Thus, it can be shown through fractography two different approaches can be used to accurately determine the critical stress intensity factor for a given mateial.

One way of determining the applicability of a particular technique is to see how well the data fits a known theoretical model. This was done for Equation 3 by plotting fracture stress vs $1/\sqrt{c}$ in Figure 5. In Figure 5 the line is the result of Equation 3 and the points were derived from measurements of the fracture surfaces (Tables 1 and 2). It can be seen From Figure 5 that the data fits reasonably well to theory.

## REFERENCES


1. R. W. Rice, "Ceramic Fracture Features, Observations, Mechanisms and Uses," Fractography of Ceramics and Metal Failures, ASTM STP 827, J. J. Mecholsky, Jr., and S. R. Powell, Jr., Eds., American Society for Testing and Materials, 5-103 (1984).

2. J. J. Mecholsky, S. W. Freiman, and R. W. Rice, "Fracture Surface Analysis of Ceramics, " J. Mater. Sci., 11, 1310-19 (1976).

3. P. N. Randall, Plain Strain Toughness Testing of High Strength Metallic Materials, Ed. by W. F. Brown, Jr. and J. E. Srawely, ASTM 410, 88-126 (1966).

4. J. J. Mecholsky, S. W. Freiman, and R. W. Rice, "Effect of Grinding on the Flaw Geometry and Fracture of Glass," J. Am. Ceram. Soc., 60[3-4], 114-17 (1977).

5. J. J. Mecholsky, "Fracture Mechanic Analysis of Glass-Ceramics," Advances in Ceramics, Vol. 4 - Nucleation and Crystallization in Gasses, Am. Ceram. Soc., 261-76 (1982).

6. J. J. Mecholsky and S. W. Freiman, " Determination of Fracture Mechanics Parameters Through Fractographic Analysis of Ceramics." Fracture Mechanics Applied to Brittle Materials , ASTM 678, Ed. by S. W. Freiman, American Society for Testing andMaterials, 136-50 (1979).

7. H. P. Kirchner and J. W. Kirchner, "Fracture Mechanics of Fracture Mirrors," J. Am. Ceram. Soc., 62[3-4], 198-202 (1979).

8. Property Data, Raytheon Research Division, Waltham, MA.

## CONCLUSIONS

Fractography can be used to identify the source of failure, to determine the state of stress during fracture, and to calculate an estimate of the fracture toughness of zinc sulfide. These representative samples from Raytheon all failed from machining-type surface cracks, were residual stress-free, and had a fracture toughness of $\approx 1.1$ $MPam^{1/2}$. This later value agreed with the published values. The values of the mirror "constants", branching stress intensity constants, and mirror to flaw size ratios etablished in this study can be used later to aid in research by identifying the true stress at failure, to identify processing or handling defects and effects during production, and finally to be used as a tool in "trouble-shooting" in-service failure of manufactured parts, e.g. laser windows.

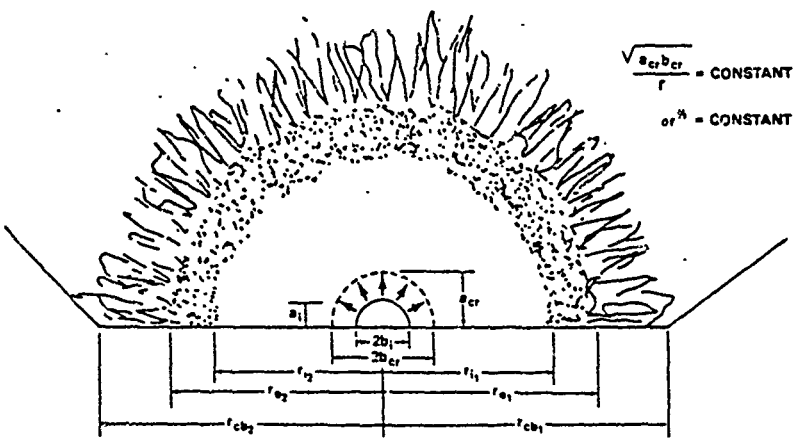


Figure 1. Schematic of the fracture surface of a brittle material subjected to a constant subcritical load. Solid semielliptical line in center represents outline of critical flaw size before catastrophic failure. Inner, $r_1$, outer, $r_2$, and crack branching, $r_{cb}$ (i.e., $r_3$), mirror radii are shown in the figure with superscript primes to indicate that there may be unsymetrical loading (Ref. 4).

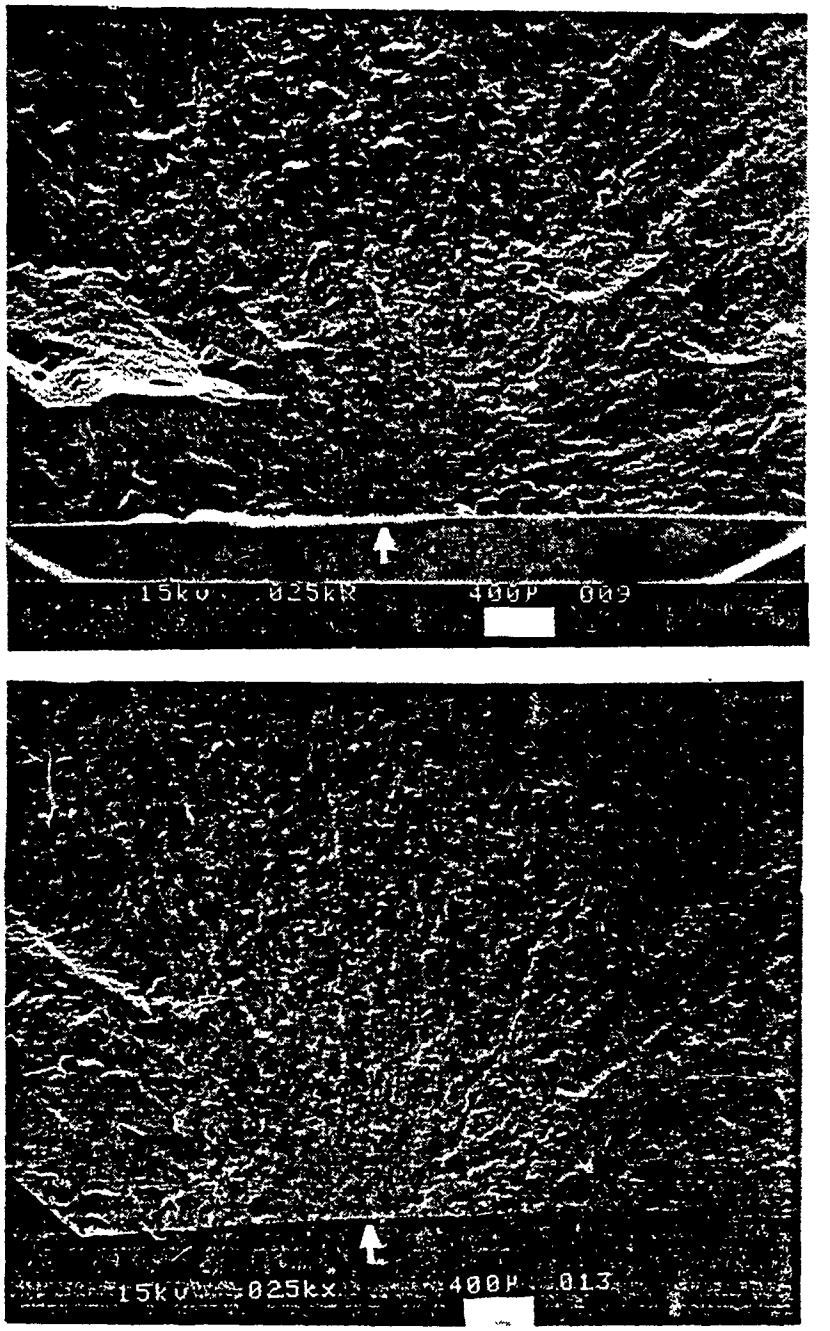


a)

b)

Fig. 2 - Fracture surfaces at low magnification (25x) with arrows indicating the position of the critical flaw along the tensile surface: a) center failure with a fracture stress of 114 MPa, b) near-center failure with a fracture stress of 108 MPa, c) corner failure with a fracture stress of 101 MPa, and d) near-corner failure with a fracture stress of 83 MPa. Bar lenth is equal to 400µm.

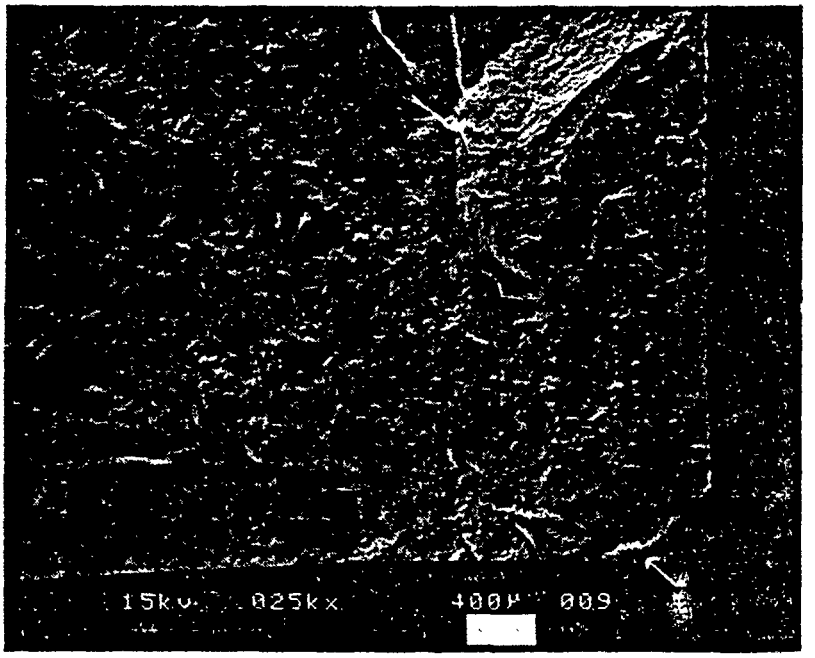


c)

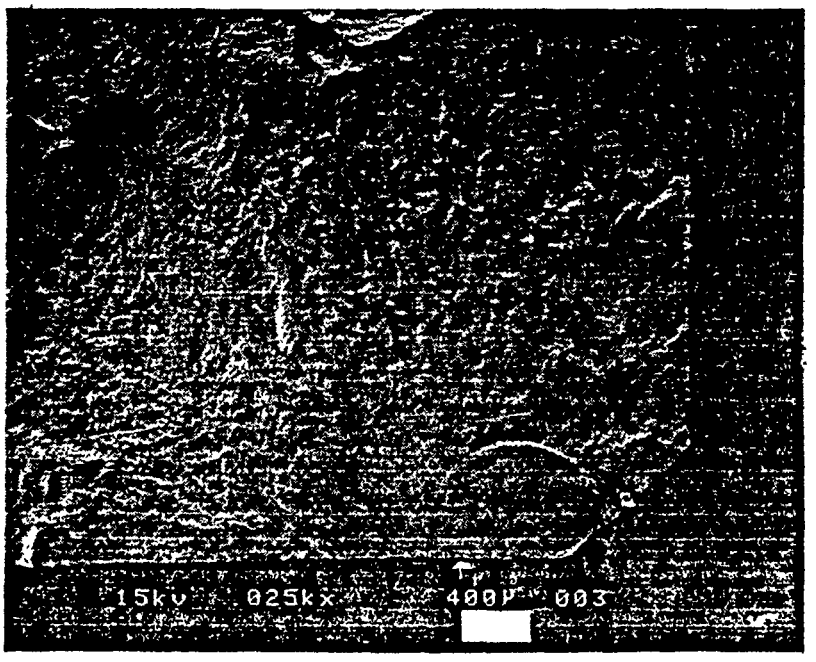


d)

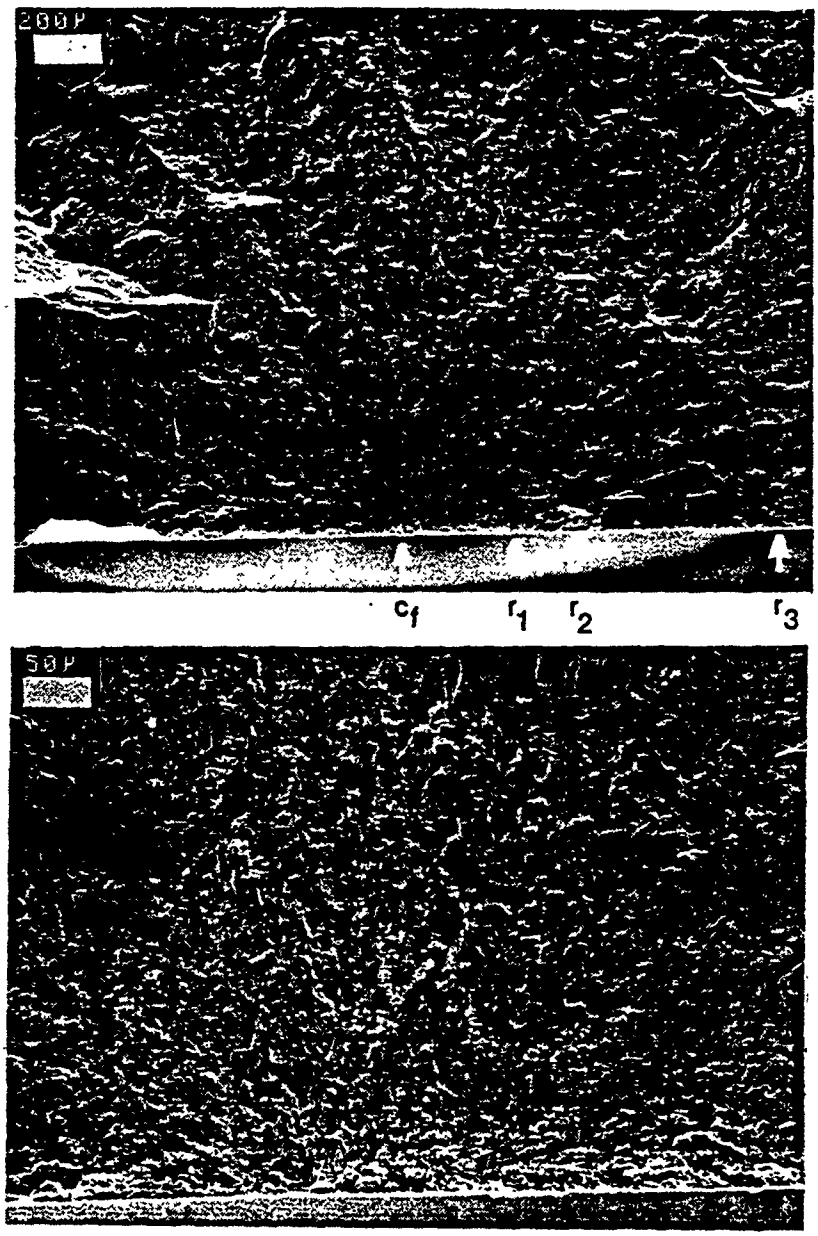


Fig. 3 - SEM micrographs of fracture surface shown in Fig. 1b) at increasing magnification: a) magnification is 50x and arrows indicate the location of the critical flaw center, inner mirror, outer mirror, and crack branching markings along the tensile surface, b) at 200x, c) at 300x, and d) at 600X with dotted line indicating the boundary of the critical flaw.

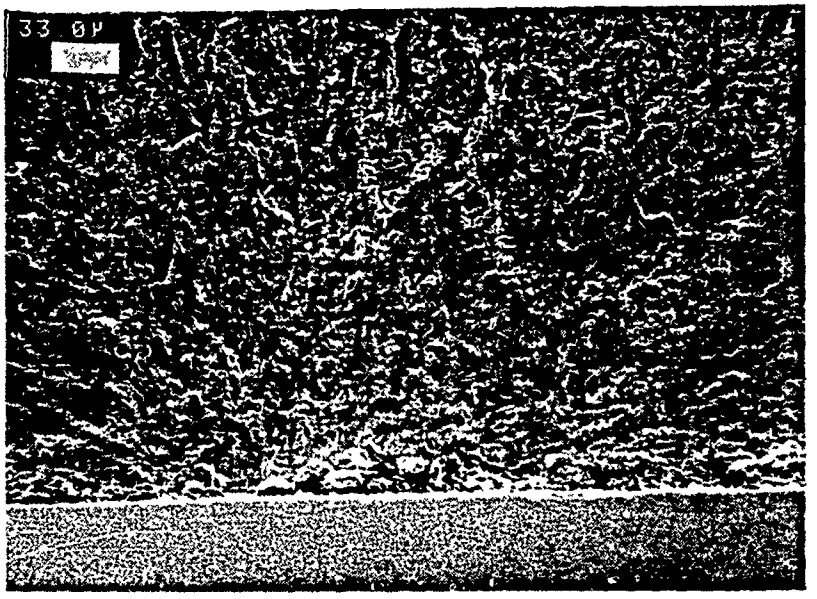


c)

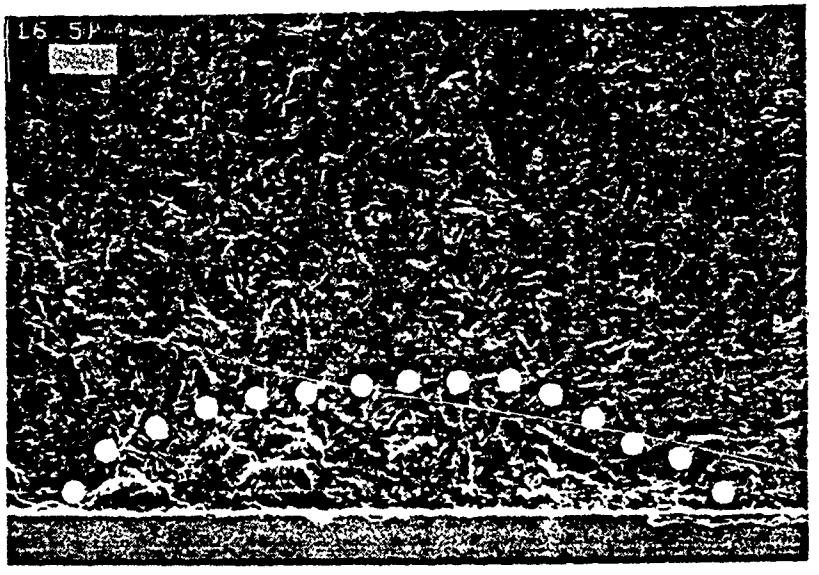


d)

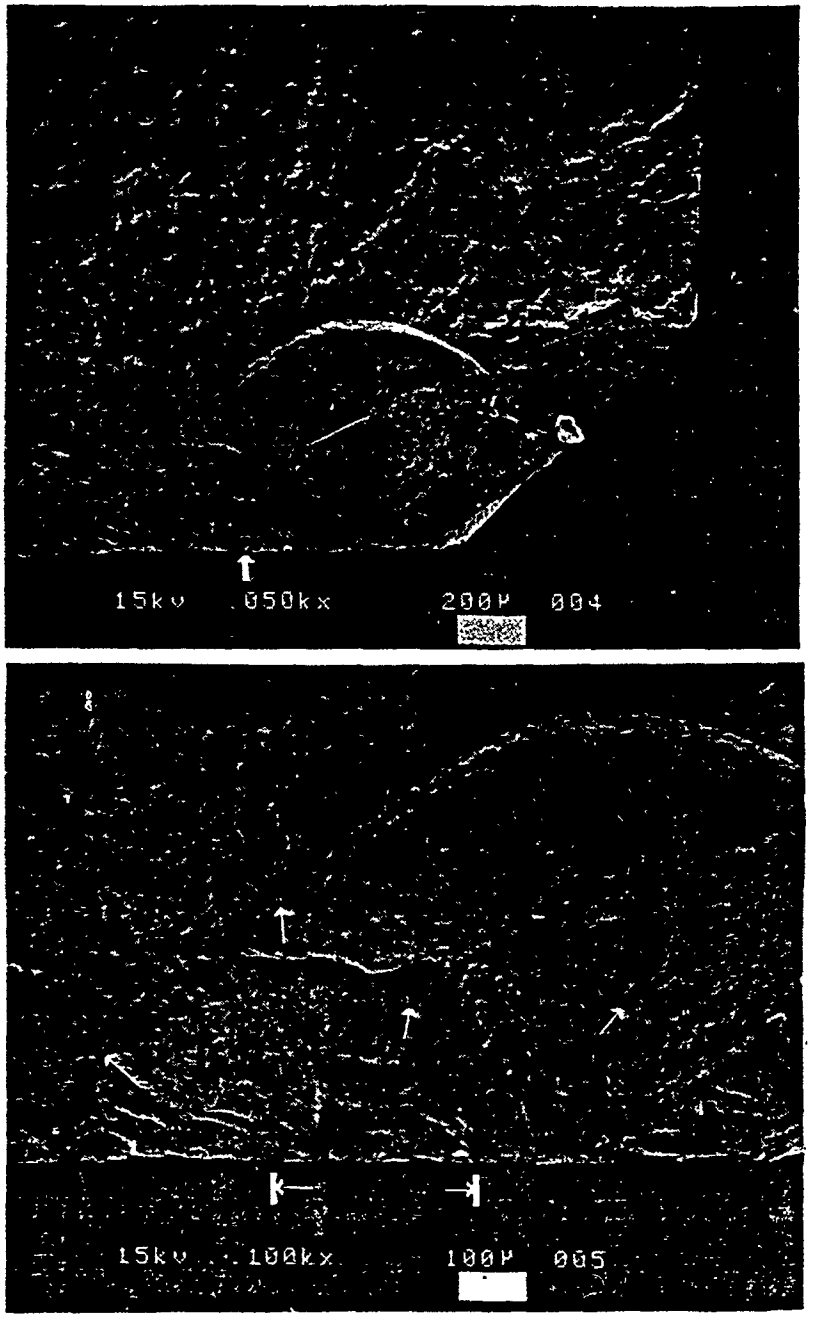


a)

b)

Fig. 4 - SEM micrographs of fracure surface shown in Fig. 1d) at increasing magnification: a) at 50x with arrow indicating the location of the critical flaw, b) at 100x with $c_f$ indicating the extent of the critical flaw along the tensile surface and the arrows in the bulk indicating the direction of fracture markings away from the point of failure, c) at 200x, and d) at 300x with the dotted line indicating the boundary of the critical flaw.

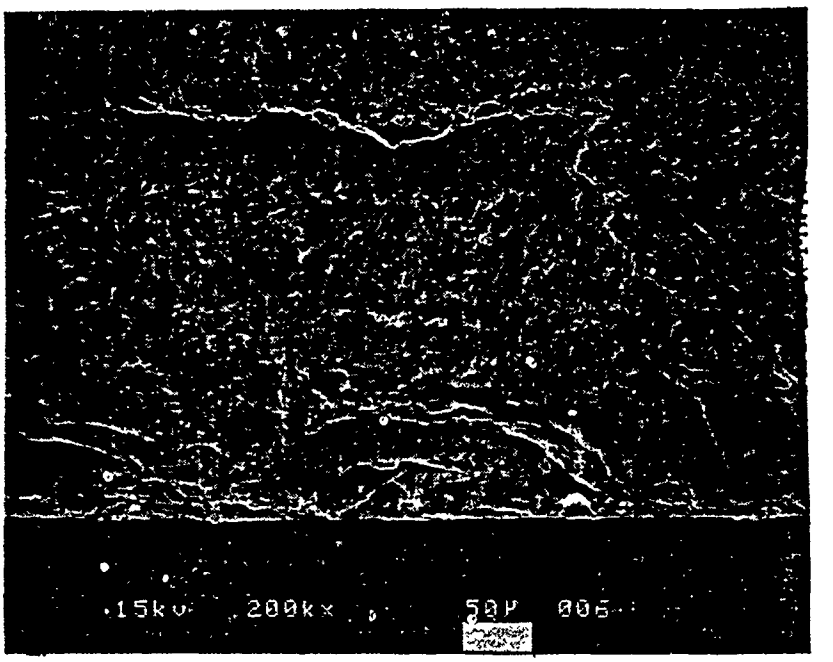


c)

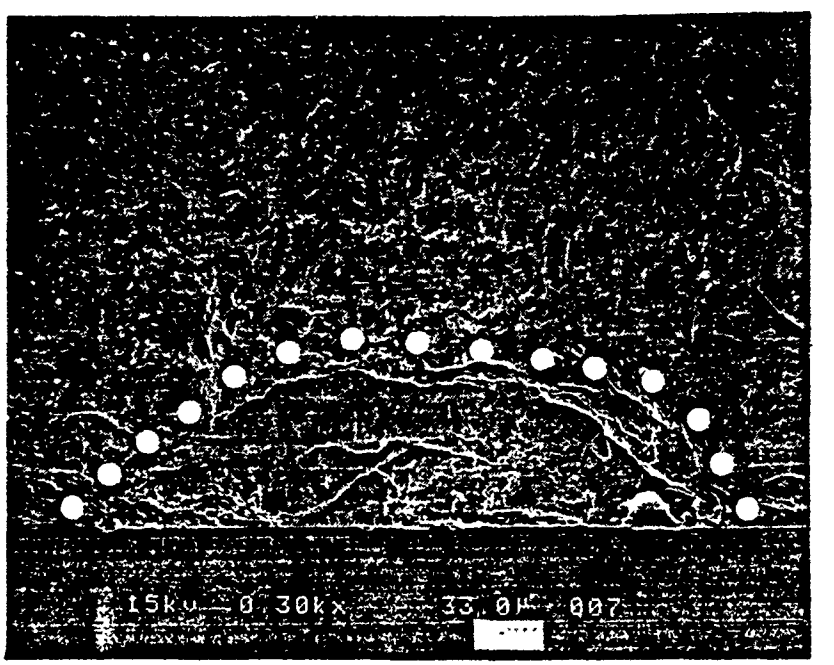


d)

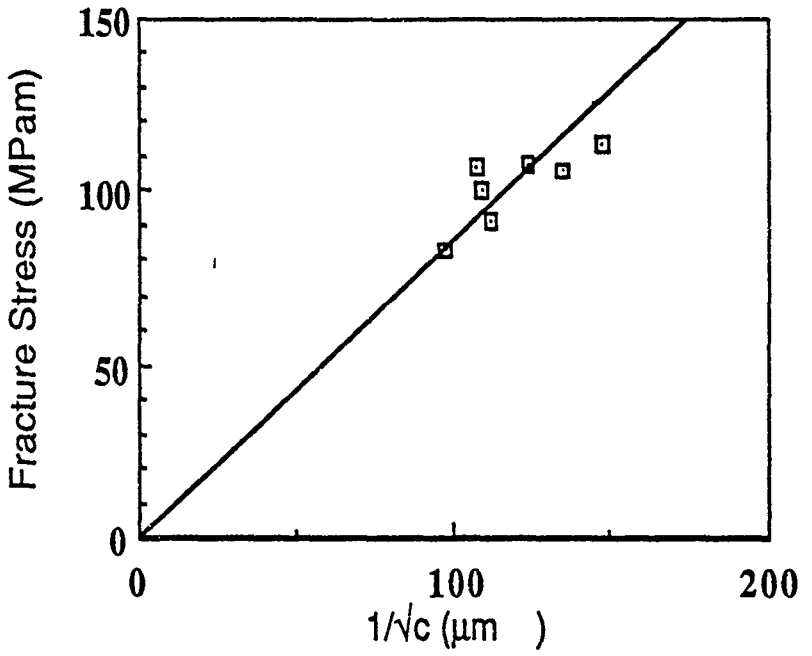


Figure 5. Plot of fracture stress vs 1/√c taken from Table 2. The solid line is the theoretical line obtained from Eq. 3 for the average stress intensity factor of the samples tested.

Table 1 - Fractographic Data for Raytheon CVD Samples

| Sample # | $r_3$ (μm) | $r_2$ (μm) | $r_1$ (μm) | a (μm) | b (μm) | c (μm) |
|---|---|---|---|---|---|---|
| 1 | 1,090 | 565 | 355 | 28.0 | 75.0 | 45.8 |
| 2 | 670 | 400 | 250 | 58.8 | 51.9 | 55.2 |
| 3 | * | 1,030 | 540 | 86.2 | 86.2 | 86.2 |
| 4 | * | * | * | * | * | * |
| 5 | 1,405 | 680 | 360 | 47.5 | 90.0 | 65.4 |
| 6 | 2,210 | 1,100 | 640 | 75.0 | 85.0 | 79.8 |
| 7 | * | * | * | * | * | * |
| 8 | 2,700 | 1,360 | 900 | 82.0 | 130.2 | 103.2 |
| 9 | 740 | 500 | 320 | 62.5 | 111.3 | 83.4 |
| 10 | * | * | * | * | * | * |

* Unobtainable due to chipping

$r_3$, $r_2$, and $r_1$ are the crack branching, outer, and inner mirror radii respectively

a and b are the depth and half-width of the critical flaw.

c is the critical flaw, $c = \sqrt{ab}$ (ref. 3)

Table 2 - Determination of Fracture Toughness

| Sample # | $\sigma_f$ (MPa) | c (μm) | $K_{IC}$ (MPam$^{1/2}$) |
|---|---|---|---|
| 1 | 114 | 45.6 | 0.95 |
| 2 | 106 | 55.2 | 0.97 |
| 3 | 107 | 86.2 | 1.24 |
| 4 | 114 | * | * |
| 5 | 108 | 65.4 | 1.09 |
| 6 | 92 | 79.8 | 1.02 |
| 7 | 125 | * | * |
| 8 | 83 | 103.2 | 1.05 |
| 9 | 101 | 83.4 | 1.14 |
| 10 | 108 | * | * |
| avg | | | 1.07 |
| std dev | | | 0.10 |

$K_{IC} = 1.24\sigma_f\sqrt{c}$ (ref. 2 & 3)

where $K_{IC}$ = fracture toughness

$\sigma_f$ = fracture toughness

c = critical flaw size

Table 3 - Mirror Constants of Raytheon Samples

| Sample # | $M_3(MPam^{1/2})$ | $M_2(MPam^{1/2})$ | $M_1(MPam^{1/2})$ |
|---|---|---|---|
| 1 | 3.8 | 2.7 | 2.5 |
| 2 | 2.7 | 2.1 | 1.7 |
| 3 | * | 3.4 | 2.5 |
| 4 | * | * | * |
| 5 | 4.1 | 2.8 | 2.1 |
| 6 | 4.3 | 3.0 | 2.3 |
| 7 | * | * | * |
| 8 | 4.3 | 3.1 | 2.5 |
| 9 | 2.7 | 2.3 | 1.8 |
| 10 | * | * | * |
| avg. | 3.7 | 2.8 | 2.1 |
| std dev | 0.7 | 0.5 | 0.3 |

* Unobtainable due to chipping and blow out

$M_j = \text{constant} = \sigma_f r_j^{1/2}$ (ref. 5)

where $M_j$ = corresponding mirror constant

$r_j$ = corresponding mirror radii

$j = 1, 2, \text{and } 3 \leftrightarrow$ 1 = mirror/mist boundary

$\leftrightarrow$ 2 = mist/hackle boundary

$\leftrightarrow$ 3 = crack branching distance

$\sigma_f$ = fracture stress

## Table 4 - Branching Stress Intensity Factors

$K_3 = 5.2\ MPam^{1/2}$

$K_2 = 4.0\ MPam^{1/2}$

$K_1 = 3.1\ MPam^{1/2}$

$K_j = M_j/0.7$ (ref. 5 & 7) - only valid along constant tensile surface

where $K_j$ = corresponding stress intensity
$M_j$ = corresponding mirror constant
$j = 1, 2,$ and 3

Table 5 - Mirror Radii - to - Flaw Size Ratio of Raytheon Samples

| Sample # | $r_3/c$ | $r_2/c$ | $r_1/c$ |
|---|---|---|---|
| 1 | 24 | 12 | 8 |
| 2 | 12 | 7 | 5 |
| 3 | * | 12 | 6 |
| 4 | * | * | * |
| 5 | 22 | 10 | 6 |
| 6 | 28 | 14 | 8 |
| 7 | * | * | * |
| 8 | 26 | 13 | 9 |
| 9 | 9 | 6 | 4 |
| 10 | * | * | * |
| avg | 20 | 11 | 6 |
| std dev | 8 | 3 | 2 |

Table 6 - Critical Stress Intensity Factor

| j = | $K_{IC}$ ($MPam^{1/2}$) |
|---|---|
| 1 | 1.01 |
| 2 | 1.05 |
| 3 | 1.05 |

$$K_{IC} = 1.24(c/r_j)^{1/2}M_j \quad \text{(ref. 5)}$$